International Journal of Innovative Technology and Interdisciplinary Sciences
https://journals.tultech.eu/index.php/ijitis
ISSN: 2613-7305
Volume 9, Issue 1
DOI: https://doi.org/10.15157/IJITIS.2026.9.1.402-432
Received: 06.10.2025; Revised: 24.12.2025; Accepted: 18.02.2026

Research Article

Thermal Analysis of Polymeric Composite Panels for Sustainable Energy Applications

Adhurim Hoxha[1], Aurela Qamili[2]*

[1]Department of Physical Engineering, Polytechnic University of Tirana, Tirana, Albania
[2]Department of Engineering, Albanian University, Tirana, Albania
***aurelazyberaj96@gmail.com**

Abstract

Polymeric composites are ideal materials for integrated photovoltaic (PV) and building-integrated photovoltaic (BIPV) applications. They are lightweight, scalable, and exhibit tenable electrical and thermal properties. To enhance heat management and module durability, this work numerically models a multilayer PV-like structure comprising a silicon (Si) absorber, a polymeric composite insulation layer, and a glass substrate. Two potential composites, polyacrylamide–silicon dioxide (PAM-SiO_2) and polyacrylamide–boron nitride (PAM-BN), were examined as the functional back-sheet layer using COMSOL Multiphysics. Steady-state and transient one-dimensional heat transfer simulations were carried out with continuous solar irradiance (G=1000Wm^{-2}) for a duration of 1000 s, with a parameter sweep of the effective thermal conductivity (k_{eff}) of the composite. The simulations assessed surface and interface temperatures, internal heat flux, and PV efficiency using temperature-dependent performance. Results show that increasing (k_{eff}) in the PAM-SiO_2 layer improves heat dissipation but moderately raises heat losses to the substrate, offering good thermal stability for moderate-efficiency systems. In contrast, PAM–BN with its higher intrinsic thermal conductivity and dielectric safety, significantly reduces the silicon cell temperature (by 1.3 K) and enhances the PV conversion efficiency by approximately +0.66%. The comparative analysis shows that PAM-SiO_2 composites provide cost-effective thermal insulation and mechanical integrity. On the other side, PAM-BN composites deliver superior heat-spreading performance. This makes them suitable for high-power or high-temperature BIPV applications.

Keywords: Thermal Analysis; Insulator; Polymeric Composite; Energy Efficiency; Optimization.

INTRODUCTION

Polymeric composites are increasingly chosen for thermal insulation systems. They have low density, adjustable thermal conductivity, and suitability for scalable production techniques [1]. With the addition of fillers such as silica (SiO_2), these materials manifest enhanced thermal stability [2]. This makes them suitable for applications that require both controlled heat dissipation and energy retention. In particular, $PAM-SiO_2$ composites demonstrate unique behaviour. This is linked to the interface synergy between the

hydrophilic PAM matrix and the thermally stable SiO_2 filler [3]. The effectiveness of the filler depends on both its volume fraction and the quality of the matrix filler interface. It regulates phonon transport across phases and affects the effective thermal conductivity [4–6].

A polymeric composite layer offers the best of both worlds with respect to tunability and thermal stability provided by the filler, and flexibility and low intrinsic conductivity provided by PAM. This is especially useful for incorporation inside layered thermal structures such as PV module back-sheets and BIPV modules [7]. Within multilayer configurations, the composite's interfacial synergy offers controlled heat transfer. This allows the structure to operate as either a heat-spreading or a thermally insulating layer. The behaviour depends on the aimed k_{eff} range [8]. Their relevance has also been highlighted in recent work on solar-driven thermal management. In this context, materials that can support energy-efficient cooling and regulating heat flow within building-integrated systems are increasingly recognized as essential components for improving overall system performance. Architectures designed to reduce cooling loads through passive heat regulation require thermally adaptive materials to provide sustainable energy systems. [9]. Such composites support broader strategies in solar-driven and energy-efficient building technologies. All this is enabled by controlled heat retention or dissipation,

Experimental observations indicate that $PAM - SiO_2$ hybrid materials show a thermal decomposition near 196 °C. Multiple degradation stages are associated with amide group scission and polymer backbone cleavage. This behavior implies adequate thermal stability for applications involving low to moderate temperatures [8]. In related systems, thermal conductivity enhancements of up to 67 % (from 0.14 to 0.24 $W\ m^{-1}\ K^{-1}$) have been reported for epoxy/$MWCNT@SiO_2$ composites at just one weight percent loading [6]. This demonstrates the importance of interface engineering even at low filler concentrations. Although not identical in chemistry, such findings provide a benchmark for $PAM - SiO_2$ based devices following similar composite design principles [10].

Furthermore, the literature distinguishes three groups of polymer-based nanocomposites: all-solid composites, foams, and syntactic foams. Thermal conductivity varies with class, ranging from ultra-insulating nanofoams (~0.0015 $W/m \cdot K$) to solid composites tailored for strength plus thermal resistance [10]. Thermal transport is primarily reduced in these systems by increasing phonon scattering via filler dispersion and interfacial mismatch, which is especially key in amorphous polymers, such as PAM [11].

System-level cooling solutions such as air ventilation, water circulation, and phase-change materials, which are often more complex and may involve additional components, are the target of recent literature reviews on solar thermal management [12]. Although these methods can successfully lower operating temperatures, they offer little information on how polymeric encapsulation or back-layer materials function as passive thermal regulators in BIPV devices. Specifically, there are still a few quantitative numerical studies

that isolate the impact of effective thermal conductivity of the composite on PV temperature and efficiency. Passive polymer composite fillers are rarely compared in PV/BIPV research employing a combined PV-electrical and building heat-flux measure under the same boundary circumstances. Additionally, the trade-off between heat dissipation and building energy retention is rarely discussed in previous research. Also, there is a lack in region-specific environmental restrictions pertinent to Mediterranean and Balkan BIPV applications considered.

Research on building-integrated photovoltaics highlights façade layout, ventilation tactics, and architectural design as the main ways to reduce heat buildup in PV modules [13]. Nevertheless, these methods mainly overlook the BIPV stack's polymeric composite layers' function as active temperature control components. Specifically, there are no published quantitative numerical studies that look at how changes in the effective thermal conductivity of polymer-based layers affect heat transport into the building and solar efficiency. It does not clearly explain the balance between improving PV cooling performance and the resulting reduction in building energy retention. Through a comparative numerical analysis of PAM-based composite layers, the current study seeks to close this significant gap in material-level modelling and building-oriented energy measures, particularly for warm-climate BIPV applications.

The use of carbon-based fillers to maximize thermal conductivity for electronics and heat-dissipation applications is the main focus of recent publications on polymer composite thermal management [14]. Although filler dispersion, percolation, and interfacial thermal resistance are important topics covered by these studies, they mainly ignore application-specific needs, including electrical insulation, multilayer behavior, and building-integrated energy systems. Specifically, compared to carbon fillers, electrically insulating fillers like SiO_2 and BN, which are essential for photovoltaic safety, remain understudied. Furthermore, the dual function of polymer composites as insulating or heat-spreading layers inside multilayer structures is not covered by current research. The necessity for comparative research specific to PV and BIPV thermal control is highlighted by the absence of application-driven modeling and system-level evaluation.

Building on these insights, this work extends the analysis beyond $PAM - SiO_2$ to include polyacrylamide–boron nitride ($PAM - BN$) composites, which have recently attracted attention for their high intrinsic thermal conductivity and excellent dielectric properties [15]. Boron nitride (BN) offers an order-of-magnitude higher thermal conductivity than SiO_2. However, it remains electrically insulating, making it a superior material for heat-spreading layers in thermally stressed PV modules [16, 17]. The comparison of $PAM - SiO_2$ and $PAM - BN$ within an identical multilayer PV-like model allows this study to investigate how filler type and k_{eff} influence the temperature distribution. Transient thermal response, and the overall insulating versus heat-dissipating behaviour of the composite layer are also evaluated.

This work examines PAM-based polymeric composites as tenable thermal layers to address the mentioned gaps in the current state of the art. The study offers a systematic

numerical comparison between insulating ($PAM - SiO_2$) and heat-spreading ($PAM - BN$) configurations within a single multilayer photovoltaic framework. This method bridges materials-level thermal design with PV performance considerations. The study considers these three hypotheses based on the mentioned gaps:

H1: The $PAM - BN$ composite layer is anticipated to lower the operating temperature of the silicon cell compared to $PAM - SiO_2$. It has a higher effective thermal conductivity and reduced interfacial thermal resistance. Improved heat dissipation is likely to improve the photovoltaic electrical efficiency under identical irradiance conditions.

H2: We predict that $PAM - SiO2$ will optimize retained energy by reducing downward heat flux due to higher interfacial scattering. Also, $PAM - BN$ will increase PV electrical output by approximately 0.5% via lower cell temperature (enhanced through-thickness heat dissipation).

H3: The $PAM - BN$ composite will likely demonstrate smoother through-thickness temperature gradients than $PAM - SiO_2$. Since it improves phonon conduction routes, it will result in quicker thermal equilibration throughout the multilayer panel.

The following sections present a numerical analysis performed in COMSOL Multiphysics. The study appraises the through-thickness temperature field, time-dependent thermal evolution, and the impact of effective conductivity on thermal regulation for both composite configurations.

MATERIALS AND METHODS

Panel Structure

The multilayer PV panel structure was simulated using COMSOL Multiphysics. The simplified two-dimensional model consists of three primary layers. The first one is a top silicon (Si) layer representing the active cell. The middle layer is the polymeric composite insulation layer, and a bottom glass substrate providing mechanical support. Each layer contributes distinctly to the system's overall thermal behaviour. The middle layer is the main focus of this investigation.

$PAM - SiO_2$ and $PAM - BN$ were analysed as materials for the middle layer. Both systems are based on a hydrophilic PAM matrix. It is selected for its low intrinsic thermal conductivity (~0.2 $W\,m^{-1}\,K^{-1}$) [5, 6], good processability, and congruence with various inorganic fillers. The $PAM - SiO_2$ composite was modelled to evaluate the effect of silica (SiO_2) nanoparticles. They are widely used in polymer nanocomposites to improve thermal resistance, interfacial adhesion, and mechanical strength [15-23]. On the other hand, the $PAM - BN$ configuration incorporates BN particles. They are known for their exceptionally high thermal conductivity, chemical stability, and dielectric properties [18, 19].

Filler-dependent heat transport mechanisms within the polymer matrix are evaluated for both mechanisms. $PAM - SiO_2$ represents a cost-effective, thermally stable insulating layer. $PAM - BN$ offers a high-performance, heat-dissipating alternative suitable for thermally stressed PV or BIPV modules. The simulations capture the influence of each

composite on temperature gradients, heat flux continuity, and steady-state thermal equilibrium across the multilayer panel.

The panel represented the system's vertical profile. It was designed as a rectangular 2D cross-section, see Figure 1.

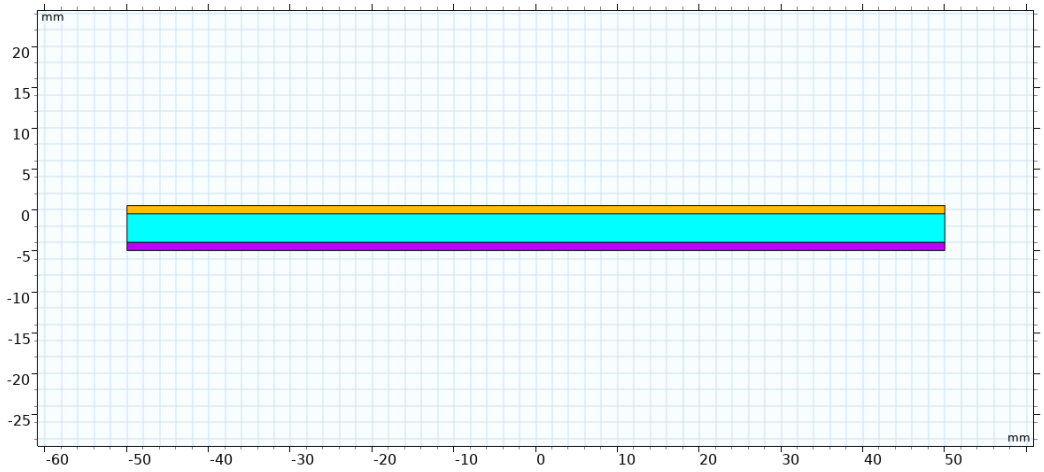

Figure 1. The representation of the panel from a rectangular 2D cross-section

The geometry has a 5.5 mm total thickness. It is divided into three layers as:

1. The middle composite layer occupies the central part (3.5 mm). It is positioned between two thinner external layers.
2. The top silicon layer (1 mm thick) is selected for its ability to absorb and distribute incoming thermal loads.
3. The bottom glass layer (1 mm thick) provides structural stability. It simulates a typical insulating base or building surface.

This layering technique is similar to methods employed in multilayer thermal insulation systems. They balance mechanical and thermal performance by sandwiching a functional composite core between structural and thermally active outer layers [20]. A 2D cross-section of a large-area panel is represented by the numerical model. Based on this, out-of-plane edge effects are neglected, which is appropriate when lateral temperature gradients are minimal.

Each layer in COMSOL was explicitly assigned to a distinct domain, allowing for the assessment of temperature, boundary interactions, and specific material properties across interfaces. In the parametric sweep, the thermal conductivity of the composite layer is considered a variable. This method allows the simulation of various composite calculations or filler concentrations.

The model extends over the entire composite height in the y-direction. Its centre is located along the vertical axis (x=0). The panel's thermal distribution is made easier by the cutline and through-thickness analysis. Furthermore, gradients are available across all materials and interfaces.

The $PAM - SiO_2$ and $PAM - BN$ layers' heat conductivity is treated as a variable by the parametric sweep.

COMSOL Setup

The multilayer panel's thermal performance under transient conditions was assessed using COMSOL Multiphysics's Heat Transfer in Solids physics interface. This module is ideal for simulating time-dependent conduction events in solid domains because it gives control over boundary interactions and thermal properties [21].

The simulation time range was used to represent the system's thermal progression under continuous heating from 0 to 1000 seconds. The geometry was built as separate domains. A user-defined mesh was applied to precisely capture steep temperature gradients. The mesh has localized refinement concentrated at all material interfaces and within the polymeric composite layer, see Figure 2. The maximum element size was set at 0.06 mm, and the minimum element size was set at 0.002 mm. This ensures numerical stability and dependable resolution of interfacial heat-transfer effects.

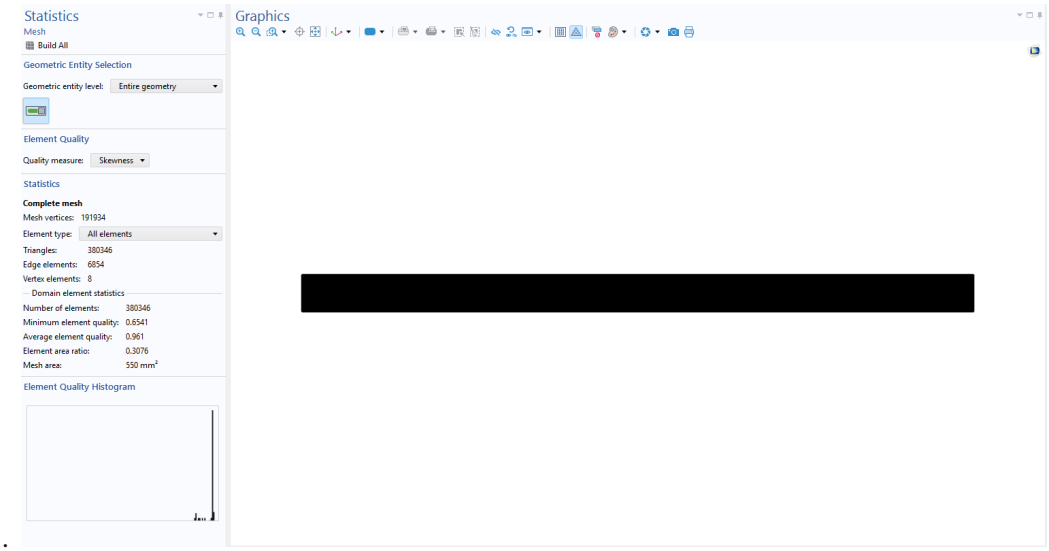

Figure 2. Mesh Statistics

The following boundary conditions were used:

- A constant heat flux of 1000 W/m^2 was applied at the upper boundary for the continuous and steady thermal load. When evaluating thermal insulation and surface heating, where energy enters the system gradually, this condition is frequently used [18].
- A convective cooling barrier was fixed at the bottom boundary to replicate natural heat exchange with the surroundings. It was performed utilising a convective heat transfer coefficient h. Thermal insulation is assessed by utilising this condition. It simulates real heat transfer from the surface to the ambient air [22].

The convective heat transfer coefficient and solar irradiance were employed as spatially uniform boundary conditions. Shading non-uniformities and wind-driven fluctuations were not considered [22].

The governing heat transfer equation in COMSOL for solid materials is derived from Fourier's law of thermal conduction via equation (1):

$$\rho C_p \frac{\partial T}{\partial t} = \nabla \cdot (k \nabla T) + Q \tag{1}$$

Where:

- ρ is the material density (kg/m^3),
- C_p is the specific heat capacity ($J/kg * K$),
- T is the temperature (K),
- k is the thermal conductivity ($W/m * K$),
- Q is the internal heat generation source (W/m^3).

The boundary heat flux for convective cooling is defined as equation (2):

$$q = h(T_{amb} - T) \tag{2}$$

where h is the convective heat transfer coefficient ($W/m^2 \cdot K$), T_{amb} is the ambient temperature, and T is the surface temperature.

This arrangement enables the realistic simulation of heat transfer on the multilayer panel. It also enables the detailed analysis of thermal energy transfer within the polymeric composite layer. The analysis of the $PAM - SiO_2$ and $PAM - BN$ systems provide the comparison of the insulating properties of the silica-based composite material with the heat-dissipation properties of the BN-based composite material. It also offers a comprehensive understanding of the thermal properties of the two materials.

Parametric Study of Composite

A parametric sweep analysis has been performed in COMSOL Multiphysics to analyse the influence of filler concentration on the thermal performance. The effective thermal conductivity (k_{eff}) was varied at 0.25, 0.35, 0.45, and 0.55 $Wm^{-1}K^{-1}$ for the $PAM - SiO_2$ composite layer. It represents progressive increases in SiO_2 loading within the PAM matrix. These values are in the typical range reported for silica-filled polymer composites. Improved phonon-transport at the matrix–filler interface leads to gradual conductivity enhancement with higher SiO_2 content [5, 18]. Similar increments have been experimentally observed in related epoxy/$MWCNT@SiO_2$ and $SiO_2 - HPAM$ systems. This confirms that modest filler additions can raise thermal conductivity by 40–70% [6, 10].

A similar sweep was conducted for the $PAM - BN$ system to extend the analysis. The coefficients used are k_{eff}= 1.5, 2.0, 2.5, and 3.0 $W\ m^{-1}\ K^{-1}$. These values are representative of polymer–boron nitride composites. BN's intrinsically high thermal conductivity (up to 300 $W\ m^{-1}\ K^{-1}$ in bulk form) can increase the effective conductivity of polymer matrices by an order of magnitude. At the same time, it preserves electrical insulation [15]. Reported

BN-polymer nanocomposites typically achieve k_{eff} values between 1 and 4 $W * m^{-1} K^{-1}$ at moderate filler fractions. These reports make the selected range realistic for heat-spreading applications in multilayer PV and BIPV structures [16, 17]. The lower k_{eff} range ($PAM - SiO_2$)emphasizes insulation-dominant behaviour. The higher k_{eff} range ($PAM - BN$) represents enhanced heat-dissipation conditions, which are typical of thermally conductive back-sheet materials.

Each sweep was performed under identical boundary and loading conditions. The aim is to isolate the effect of filler type and concentration on temperature distribution, interfacial thermal gradients, and surface temperature rise. The results provide direct insight into the transition from thermally insulating ($PAM - SiO_2$) to thermally conductive ($PAM - BN$) regimes. The results support optimised material selection for specific PV or BIPV operating environments.

Effective Medium Modelling of Filler Fraction Influence (Bruggeman Approach)

The composite conductivity was also interpreted using a typical effective medium theory (Bruggeman) relation for dispersed fillers to connect the simulated effective conductivity range to physically significant filler loadings:

$$\Phi \frac{k_f - k_{eff}}{k_f + 2k_{eff}} + (1 - \Phi) \frac{k_m - k_{eff}}{k_m + 2k_{eff}} = 0 \quad (3)$$

Where Φ is the filler volume fraction and k_m is the matrix thermal conductivity and k_f the filler thermal conductivity.

The obtained $k_{eff}(\Phi)$ trends for $PAM - BN$ and $PAM - SiO_2$ are shown in Figure 3. As Φ increases, the BN-filled example exhibits a noticeably stronger increase in k_{eff}, which is consistent with the formation of efficient heat-spreading channels, especially as the matrix becomes less resistive.

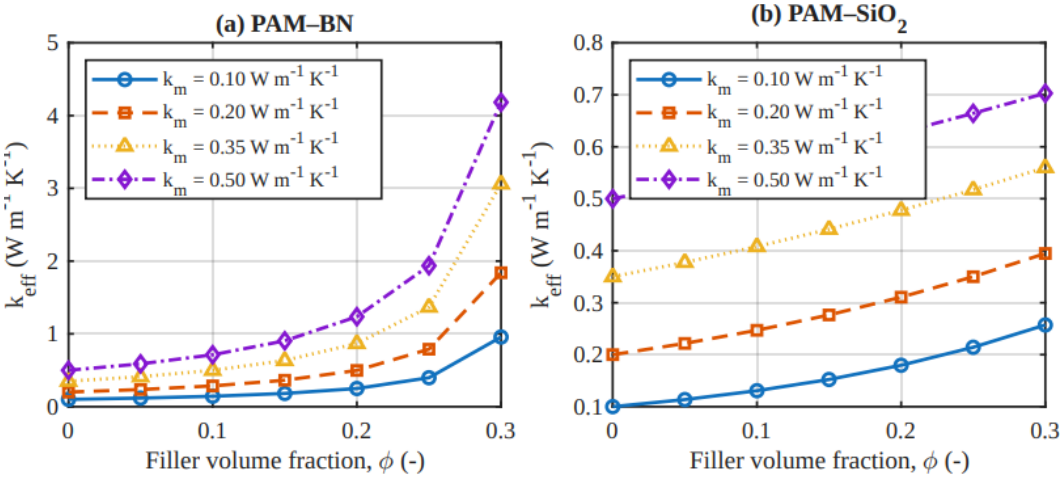

Figure 3. Bruggeman effective medium predictions of the effective thermal conductivity as a function of filler volume fraction for (a) PAM − BN and (b) PAM − SiO_2 composites.

As opposed to continuous conductive networks, the SiO_2-filled system shows a more gradual increase in k_{eff}, which is consistent with interfacial-dominated heat transport;

similar silica-based composite architectures have been shown to enhance thermal transport while preserving electrical insulation through interfacial design [6]. Without addressing filler orientation, percolation, or anisotropic transport effects, the Bruggeman formulation provides a bulk-averaged effective conductivity under the assumption of isotropic filler dispersion.

In this study, Φ was swept from 0 to 0.30, while k_m was varied (0.10, 0.20, 0.35, 0.50 $W \cdot m^{-1} \cdot K^{-1}$) to reflect matrix-property variability in polymer composite systems. For $PAM-BN$, h-BN was treated as a high-conductivity dielectric filler with a representative intrinsic k_f on the order of several hundred $W \cdot m^{-1} \cdot K^{-1}$. This matches with reports for thermally conductive BN–polymer composites [1]. The filler conductivity (around 1.3–1.4 $W \cdot m^{-1} \cdot K^{-1}$) was considered a representative bulk-like amorphous SiO_2 value for $PAM-SiO_2$ [4].

The physical foundation for understanding the effective conductivity values utilized in numerical simulations is provided by these effective medium trends. Appendix A reports a straightforward mapping between the COMSOL k_{eff} sweep and equivalent filler volume fractions derived from Eq. (3).

RESULTS AND DISCUSSIONS

Simulations were executed to evaluate the thermal response of a multilayer PV-like structure under two material choices for the middle-layer and two heat-input formulations. The middle layer was modelled as a $PAM-SiO_2$ composite and a $PAM-BN$ composite, respectively.

For each material, two cases were solved:

I. A *constant irradiance* case with G = 1000 Wm^{-2} (applied as a steady top-surface heat flux), and

II. A *temperature-coupled* boundary case in which the net top-surface heat flux was modelled explicitly as

$$q^n = \alpha G - \eta G - h_{top}(T - T_{amb}) - \varepsilon\sigma\,(T^4 - T_{sky}^4) \quad (4)$$

where α is the absorptance, η the temperature-dependent PV efficiency, h_{top} the convective heat transfer coefficient, and $\varepsilon\sigma\,(T^4 - T_{sky}^4)$ the radiative exchange term with the sky. This dual-approach framework contrasts a simplified steady input with a more realistic, self-regulating boundary condition that responds to surface temperature.

Temperature Difference (ΔT) vs k_{eff}

The parametric study's findings demonstrate an evident inverse relationship between ΔT and the thermal conductivity of the composite layer. The panel's capacity to disperse heat improves with an increase in effective thermal conductivity (k_{eff}), which in turn lowers the surface temperature after the 1000-second simulation. Figure 4(a) presents the results for the $PAM-SiO_2$ layer when k_{eff} is varied from (0.25 to 0.55 W m^{-1} K^{-1}) while Figure 4(b) illustrates the effect of thermal conductivity on ΔT. Meanwhile, k_{eff} = 1.5, 2.0, 2.5 and 3.0 W m^{-1} K^{-1} for the $PAM-BN$ layer.

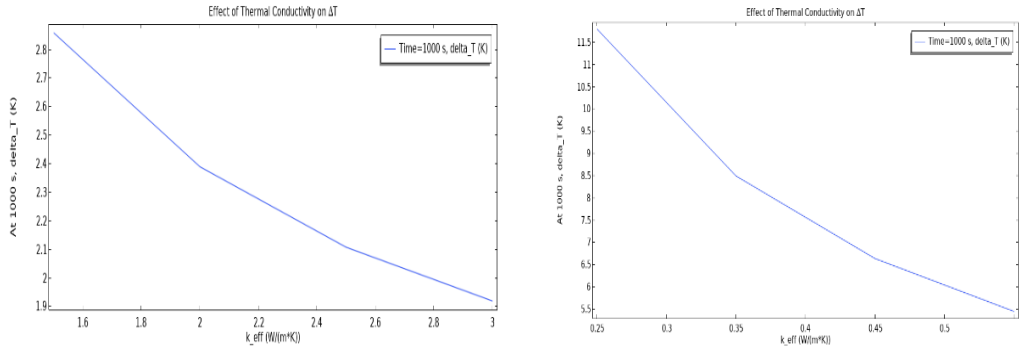

(a) (b)

Figure 4. Effect of k_{eff} on ΔT

Surface Temperature Distribution Along the Arc Length

The lateral distribution of temperature along the arc length was examined next. This helps to further understand how the temperature reduction manifests across the panel surface.

The temperature variation along the 100 mm upper surface of the panel was evaluated to understand how each composite spreads heat laterally. Figures 5(a) and 5(b) show the arc-length profiles for all effective thermal conductivities in $PAM - BN$ and $PAM - SiO_2$ at t = 600 s.

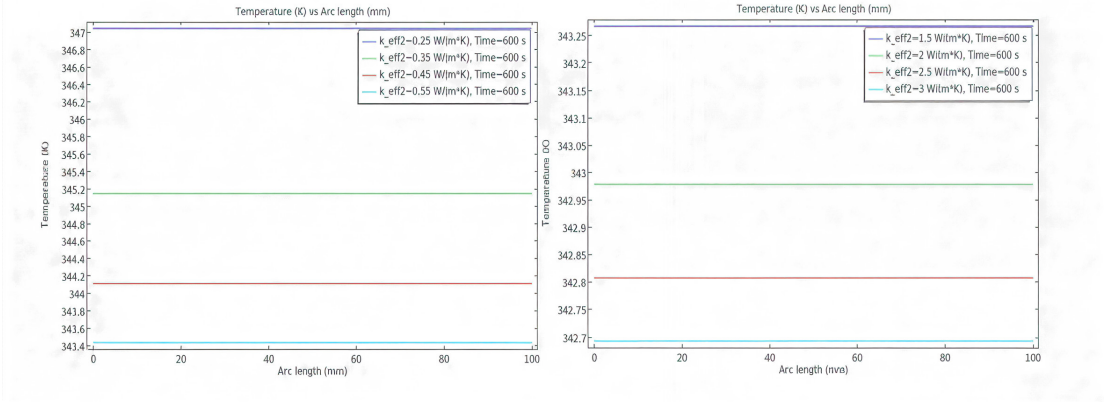

(a) (b)

Figure 5. Surface temperature profiles along the 100 mm arc length at t = 600 s

In both materials, under the chosen operating conditions, heat transfer is primarily through-thickness rather than in-plane, as seen by the relatively flat arc-length profiles and lateral variation that stays within approximately 1% of the mean surface temperature. This indicates that through-thickness gradients dominate, and 2D/3D effects become necessary primarily for small or aspect-ratio-limited panels or strong edge-loss regimes. This also indicates that heat moves vertically into the underlying layers rather than spreading

sideways. Small in-plane temperature gradients indicate that transport in the through-thickness direction is more dominant for heat transfer. This is also suggested by the guidelines for modelling layered materials in the COMSOL Heat Transfer Module User's Guide [21]. It justifies the use of the 1D conduction analysis approach.

The overall temperature level changes with thermal conductivity, even though the profiles have the same flat shape. Lower k_{eff} values show minimal higher surface temperatures. This is related to the reduced heat removal from the top layer. With the increase of k_{eff} the surface becomes cooler. This reflects the improved vertical heat spreading and faster transfer of energy toward the bottom layers.

From the comparison of the two materials, $PAM-BN$ consistently maintains lower surface temperatures than $PAM-SiO_2$ at similar conductivity values. This behaviour highlights the enhanced thermal conduction of BN-filled composites. Also reflects their ability to reduce surface overheating during continuous solar loading.

Through-Thickness Temperature Profiles

The vertical cut-line analysis was performed over the entire thickness of the panel (0-5.5 mm) for both materials. It determines the internal temperature gradient at t = 600 s for each k_{eff}. The results are shown in Figure 6(a) and 6(b).

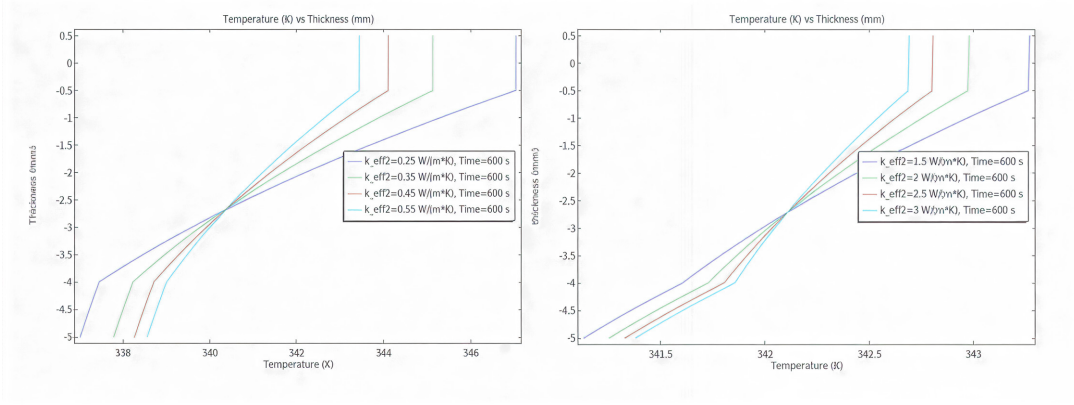

(a) (b)

Figure 6. The temperature distribution at t = 600 s for the through-thickness analysis.

The lowest conductivity (0.25 $W/m \cdot K$) for $PAM-SiO_2$ (Figure 6(a)), causes the maximum temperature difference between the top and bottom surfaces. The heat is mostly confined to the top part, while the bottom part is relatively cooler. This is due to the insulating behaviour of silica-filled PAM, which limits thermal transport and keeps heat confined near the irradiated boundary. As conductivity increases from 0.35 to 0.55 $W/m \cdot K$, the temperature profiles become smoother. Also, the difference between the top and bottom surfaces narrows. This shows that the material can conduct the heat better.

The $PAM-BN$ composite (Figure 6(b)) behaves differently. Even with the lowest conductivity of BN at 1.5 W/m·K, the temperature gradient is already more gradual compared to the SiO_2-based system. With the increase of k_{eff} to 3 $W/m \cdot K$, the temperature

gradient becomes almost linear. This indicates that heat transfer in the BN-filled layer is fast and heat is well distributed from top to bottom. $PAM-BN$ has about 20% less through-thickness temperature gradients than $PAM-SiO_2$ because of its higher effective conductivity.

By comparing these two materials, the contrast in their functions can be observed. For the same position and thickness, the BN composite material is seen to maintain the upper part at a lower temperature. Meanwhile, the temperature increases towards the bottom. This indicates that the heat is not concentrated at the surface but is rather distributed inside.

Temperature Difference (ΔT) vs Irradiance (G)

Additional simulations were performed to evaluate how the composite responds under realistic outdoor conditions. The solar irradiance is varied under three irradiance levels 600, 800, and 1000 W/m^2 to represent typical Mediterranean solar loading [23]. Figures 7(a) and 7(b) present the results for $PAM-BN$ and $PAM-SiO_2$. Representative k_{eff} values have been used for each material.

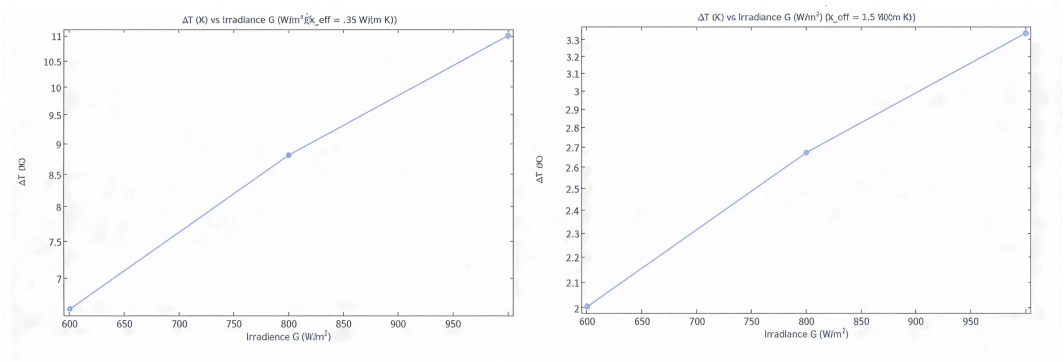

(a) (b)

Figure 7. The variation of ΔT with solar irradiance

ΔT is found to increase linearly with irradiance for both composites. This reveals that the absorbed solar irradiance is the major factor in surface heating. The irradiance sweep simulation also reveals the variation in thermal properties of both composites. ΔT increases by 66% for $PAM-BN$ (from 2.0 K to 3.33 K) compared to 65% for $PAM-SiO_2$ (from 6.65 K to 11.0 K).

The linear increase in solar irradiance (G) caused a corresponding linear increase in the temperature difference (ΔT) for both composites. This was expected by the principles of radiative loading. The ΔT values for the BN-filled system were always lower than those of the other composite at all irradiance levels, thus verifying the better heat-spreading properties of the former.

Temperature Difference (ΔT) vs Convective Cooling Coefficient (h)

The plot of temperature difference (ΔT) versus the convective cooling coefficient h reveals that ΔT rises marginally with the increase in the value of h from 10 to 25 W/m^2K. The plot

represents the dependence of ΔT on h at the steady state. As the value of h is lower, around 10 W/m^2K, the temperature difference is higher. This indicates poor heat evacuation from the system. However, as h increases beyond 16-18 W/m^2K, the temperature difference decreases substantially. This indicates efficient heat evacuation from the system. Figure 8(a) and (b) emphasize the importance of convective cooling in reducing the operating temperature and achieving a relatively equal thermal distribution in the $PAM-SiO_2$ and $PAM-BN$ layer, respectively.

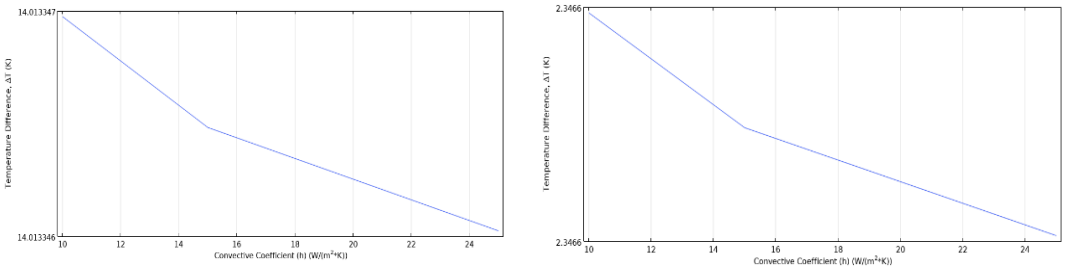

(a) (b)

Figure 8. The effect of the Cooling Coefficient on ΔT

Temperature Rise over Time

The transient response demonstrates that the system temperature rises rapidly during the initial heating period. It gradually approaches a steady-state value of about 375 K after approximately 4000 s. The curve follows an exponential trend. This is typical of thermal diffusion–controlled heating. It also confirms that the panel reaches thermal equilibrium under constant irradiance $G = 1000\ Wm^{-2}$. Figure 9(a) and (b) illustrate the stable operational temperature for the $PAM-SiO_2$ and $PAM-BN$ configuration, respectively.

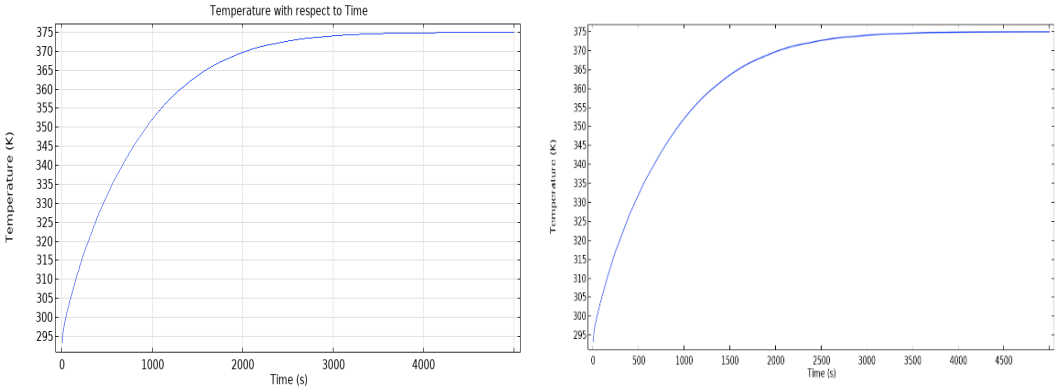

(a) (b)

Figure 9. Temperature with respect to time

Parameters with Temperature-Coupled Boundary

Table 1 shows the comparison between $PAM - SiO_2$ and $PAM - BN$. It is obvious how the filler type changes both heat flow and electrical performance in the panel. $PAM - BN$ gives a slightly higher PV efficiency (0.1735) and power output (173.5 Wm^{-2}) than $PAM - SiO_2$, mainly because its higher thermal conductivity helps the silicon layer stay cooler by about 1.3 K. A lower cell temperature improves power conversion efficiency and overall module performance.

Looking at the other parameters, this improvement comes with a trade-off. The $PAM - BN$ layer transfers more heat into the building (284.9 Wm^{-2}) compared to 267.0 Wm^{-2}), which means it provides less insulation. As a result, the net retained energy is lower for $PAM - BN$ (78.5 Wm^{-2}) than for $PAM - SiO_2$ (83.4 Wm^{-2}).

Table 1. Parameters from the Conduction Model

Metric	PAM–SiO_2	PAM–BN	Difference (BN vs SiO_2)	Result
PV efficiency	0.17236	0.17350	+0.00114 (~ +0.66%)	BN cools the cell slightly, leading higher η.
Bottom temperature (K)	328.86	327.59	−1.27 K	BN conducts heat better, leading cooler module.
PV Power output (Wm^{-2})	172.36	173.50	+1.14	Follows η: BN gives more electrical power.
Heat flux to building (Wm^{-2}))	267.01	284.89	+17.88	BN's higher k_{eff} sends more heat into the building (less insulation).
Net energy (Wm^{-2})	83.359	78.542	−4.817	SiO_2 retains more total energy (better insulation).

Following our simulation outputs, the net retained energy was defined as the difference between PV electrical power and the downward heat flux, as seen below:

$$E_{net} = q_{PV} - q_{loss} \quad (5)$$

where q_{PV} is the useful electrical power generated by the PV module (Wm^{-2}), and q_{loss} is the downward heat flux entering the building (Wm^{-2}). This metric is introduced here to quantify insulation performance under identical boundary conditions.

Using the simulated values, we can have $E_{net}^{SiO_2}$=172.36−267.01=−94.65Wm^{-2} and E_{net}^{BN}=173.50−284.89=−111.39Wm^{-2}. The relative retained energy advantage of PAM-SiO2 is then $\Delta E_{retained}$= $E_{net}^{SiO_2}$-E_{net}^{BN}=16.74Wm^{-2}.

This value highlights that the SiO_2-filled composite retains 16.74 Wm^{-2} more usable energy than the BN-filled system under identical conditions. When extrapolated to typical rooftop PV installations in Albania (1.5–3 kW systems) [24], this difference corresponds to 25–50 W of avoided thermal loss per module, directly supporting national goals for improved building energy efficiency.

The current study shows that passive polymeric composite layers alone can cause quantifiable energy-flow redistribution inside the PV stack, whereas many PV/T solutions described by [2] rely on active cooling or fluid-based heat extraction to improve performance.

Theory and Validation

Another variable to be considered in multilayer PV/BIPV stacks is the additional thermal boundary resistance at solid–solid interfaces that can introduce an extra temperature drop and reduce the apparent heat transfer rate. [4] discovered that an additional thermal resistance at interfaces, such as dielectric or substrate assemblies, influences the apparent thermal conductivity, and that the thickness effects in SiO_2 thin films can be explained by this interface resistance. The Si/composite and composite/glass interfaces can be described in a compact analytical model by an interfacial resistance R_K, which generates an interfacial temperature difference proportionate to the through-thickness heat flux. This makes it possible to clearly distinguish between bulk conduction and interface-limited transport in the theoretical model. The Kapitza resistance represents the interface between adjacent layers to account for this effect in an analytical form, see equation (6):

$$\Delta T_{int} = q'' R_K \tag{6}$$

where q'' is the heat flux (W·m^{-2}) and R_K is the interfacial thermal resistance (m^2·K·W^{-1}). The total thermal resistance across a single composite layer enclosed by two surfaces under steady-state one-dimensional conduction can be expressed as follows:

$$R_{tot} = \frac{L}{k} + R_{K,1} + R_{K,2} \tag{7}$$

leading to the heat-flux expression:

$$q'' = \frac{\Delta T}{R_{tot}} \tag{8}$$

While the effective thermal conductivity parameter used in the numerical model captures the dominant trends, interfacial resistance is conceptually discussed in the current study to support the theoretical framework and explain observed differences in effective thermal behaviour between PAM–SiO_2 and PAM–BN systems.

The current method does not specifically address phonon routes at the nanoscale, in contrast to previous experimental investigations on thermally enhanced polymer composites, such as the silica-coated MWCNT epoxy systems described by [6]. Rather, by including interfacial thermal resistance effects into a macroscopic conduction framework, it enhances these investigations by allowing direct comparison of two dielectric fillers under the same PV-relevant boundary conditions. While [6] demonstrated experimentally that interfacial engineering can significantly enhance heat transport, the present model translates these interfacial phenomena into effective thermal behaviour suitable for system-level PV and BIPV thermal analysis.

The current model does not account for possible moisture absorption or humidity-induced modifications in PAM characteristics. As a result, the findings reflect dry-state thermal behavior and could change after extended exposure to a high-humidity environment.

The analytical validation is based on a one-dimensional conduction model that assumes negligible lateral heat losses, which is appropriate for large-area PV panel structures where in-plane gradients are minimal. Material properties are considered constant, and the boundary conditions reflect the steady-state irradiated scenario employed in the simulations. Over the examined temperature range, the material's thermophysical characteristics were considered consistent and stayed well below the PAM-based composites' degradation thresholds. These assumptions are necessary for a consistent comparison between the analytical and numerical models.

Comparison between theoretical and simulated results reveals excellent agreement between them. Errors less than 0.05% are calculated for both composites. This is an extremely small deviation, which verifies that the COMSOL simulation is correctly solving the steady-state conduction equation.

$$\Delta T_{theory} = q''\left(\frac{L_{Si}}{k_{Si}} + \frac{L_{comp}}{k_{eff}} + \frac{L_{glass}}{k_{glass}}\right) \quad (9)$$

where q''=1000 W/m^2, L_{Si}=1 mm, $L_{composite}$=3.5 mm, L_{glass}=1 mm, k_{Si}=148 $W/m.K$, and k_{glass}=1.0 $W/m.K$.

$$Error\ (\%) = \frac{(\Delta T_{COMSOL} - \Delta T_{Theory})}{\Delta T_{Theory}} \times 100 \quad (10)$$

Table 2 depict the error percentage

Table 2. Error Percentage

Composite	ΔT_{Theory} (K)	ΔT_{COMSOL} (K)	Error (%)
PAM–SiO_2	11.01	11.006	0.036%
PAM–BN	3.34	3.339	0.030%

The temperature difference in the $PAM - BN$ composite is smaller because of its higher thermal conductivity. It improves the heat transfer in the layer. Conversely, $PAM - SiO_2$

has a slightly higher temperature gradient because of its lower k_{eff}, which confirms its higher insulating property.

The reduced-order analytical solution of the one-dimensional heat conduction problem was employed as a reference to further test the transient solution obtained in the numerical simulations. The time course of the spatially averaged temperature rise was modeled by the dominant diffusion-controlled mode of the 1D heat equation instead of incorporating another physical model.

The transient response of the panel can be expressed as $\Delta T(t) = \Delta T^{\infty}(1 - e^{-t/\tau})$ under constant boundary conditions. ΔT^{∞} is the steady-state temperature rise and τ represents the effective thermal time constant. This closed-form solution is the leading eigenmode of the 1D heat equation. It serves as a compact analytical model for conduction-dominated transient problems. The analytical solution was directly fitted to the COMSOL-exported transient temperature solutions for both composites. The fitted parameters and associated error measures are listed in Table 3.

Table 3. Analytical transient validation metrics

Composite	ΔT^{∞} **(K)**	$\tau(s)$	**RMSE (K)**	**RMSE (%)**	$\boldsymbol{R^2}$
PAM–BN	82.236	775.59	0.596	0.72	0.99899
PAM–SiO_2	82.239	775.65	0.584	0.71	0.99896

The analytical and numerical results showed excellent agreement, with relative errors staying below 1% over the whole transient period and coefficients of determination reaching 0.998. The tight match demonstrates that the primary diffusion-controlled thermal response of the composite panels is accurately captured by the COMSOL simulations. While the improved thermal performance of BN-filled systems is reflected in lower temperature gradients and improved heat-spreading efficiency rather than changes in the global time constant, the nearly identical values of ΔT^{∞} and τ observed for PAM–BN and PAM–SiO_2 show that the global transient response is primarily governed by panel geometry and boundary heat exchange.

To assess the robustness of the numerical results with respect to temperature-dependent transport effects reported in the literature, a bounded sensitivity analysis was performed by perturbing the effective thermal conductivity k_{eff} within a ±10% range. The ranges are consistent with reported values for polymer-based thermal management materials over the relevant operating temperature interval [1].

The resulting variation in the effective thermal time constant τ and transient temperature evolution was evaluated using the reduced-order analytical transient formulation, without changing the numerical model or boundary conditions. As predicted for diffusion-dominated heat transport, a ±10% change in k_{eff} causes an asymmetric fluctuation of the global time constant, with τ rising by around 11% for decreased conductivity and falling by about 9% for higher conductivity. Throughout the whole duration, the resulting variation in the transient temperature response is limited. The

transient response is particularly sensitive to changes in the effective thermal time constant during intermediate times (about 1000 s), when the maximum envelope difference, normalized with respect to the steady-state temperature rise, is about 3.8%. As time progresses, this deviation decreases rapidly, falling below 0.2% at long times as the system approaches steady state. For both PAM–BN and PAM–SiO_2 composites, nearly comparable sensitivity limitations are found, suggesting that reasonable temperature-induced changes in the effective thermal conductivity k_{eff} do not affect the global transient thermal response as reported also from [4].

Additionally, a combined sensitivity and uncertainty analysis was conducted to assess the model's robustness. To measure the effect of parameter variability on the simulated temperature rise, a ±10% perturbation was given to the convection coefficient and effective thermal conductivity. The coefficient of variation of the temperature rise for differences in effective thermal conductivity ranges from 3.25% to 5.81%, with a maximum standard deviation of 0.50 K, according to Monte Carlo uncertainty propagation (N = 50,000) based on response maps obtained using COMSOL. Conversely, the convection coefficient uncertainty leads to a maximum standard deviation of 0.093 K and a coefficient of variation between 0.41% and 1.06%. While the overall scope of the uncertainty stays confined and does not change the comparative thermal trends mentioned in this work, the thermal response is far more sensitive to changes in effective thermal conductivity than to convective boundary conditions.

These results confirm that the constant-property assumption adopted in the simulations is appropriate for the present analysis and that the comparative thermal performance conclusions are robust with respect to temperature-dependent uncertainties reported in state-of-the-art studies.

SOTA

The development of thermally optimized polymeric composites has become a major focus in PV and BIPV research. Recent research has shown that the thermal conductivity of polymer composites is highly dependent on the type of filler, filler volume fraction, and phonon coupling at the interfaces [25, 27]. Silica fillers are low cost and enhance stability and insulation [28]. Alumina fillers offer a good balance between conduction and insulation, and boron nitride fillers have exceptional thermal conduction properties with good electrical insulation.

Table 4. SOTA Comparison

Composite	k_f ($W \cdot m^{-1} \cdot K^{-1}$)	k_{eff} ($W \cdot m^{-1} \cdot K^{-1}$)	ΔT_{Theory} (K)	Efficiency Gain (%)	Cost /W	SOTA	Limitations	Ref
PAM–SiO_2	1.4	0.35	11.01	Baseline	Low	Amorphous SiO_2 introduces strong	Limited heat spreading; unsuitable	[4, 5, 26]

						phonon scattering; heat is carried mainly by non-propagating modes (diffusons).	for high-heat PV	
PAM–BN	200–400	1.50	3.34	+0.66 (this work)	High	Formation of continuous, high-conductivity phonon pathways; reduced interfacial resistance relative to oxides.	Dispersion sensitivity; higher material cost	[4, 14]
PAM–Al_2O_3	25–30	0.85	5.85	~0.3–0.4	Low - Moderate	Ceramic fillers improve bulk conduction but require high loading to form conductive pathways.	High filler loading increases brittleness and density.	[2, 23, 27]
PAM–MWCNT@SiO_2	3000 (CNT core), but the silica shell limits conduction	0.24	7.00	~0.4–0.6	High	CNT cores offer high phonon transport; SiO_2 shell reduces interfacial mismatch and electrical risk.	Dispersion, alignment, and cost strongly limit scalability.	[6, 14]
HPAM–SiO_2 (Oil Recovery Variant)	1.4	0.20–0.30	12–15	Not reported	Low	Composite optimized for viscosity and salinity	Optimized for rheology, not thermal management	[7, 27]

						tolerance, not for phonon transport.	; low k_{eff} for solar applications.	
Pure PAM	0.20(matrix only)	0.20	14.68	Not Reported	Very Low	Heat transport dominated by amorphous polymer chains; negligible phonon propagation.	Very low thermal conductivity; moisture sensitivity.	[3, 5]

The design of thermally optimized polymeric composites has emerged as a prominent theme in PV and BIPV materials science. As has been discussed in a number of research papers, the thermal properties of polymeric matrices are highly sensitive to the nature of fillers, filler fraction, intrinsic conductivity, and the extent of phonon coupling at the matrix/filler interface [1, 6, 10]. Silica-based fillers (SiO_2) are generally known to improve insulation and thermal resistance at a low cost. This makes them suitable for passive thermal barriers [2, 3]. Alumina (Al_2O_3) systems provide an intermediate property, which offers moderate improvements in conduction with good electrical resistance. This makes them suitable for PV modules exposed to fluctuating thermal conditions [27].

Boron nitride (BN) is remarkable for its unique combination of high intrinsic thermal conductivity and high dielectric strength. These properties enable efficient heat dissipation without compromising electrical safety, a critical concern for high-voltage PV and BIPV applications. [15, 16] This is significant because, unlike Al_2O_3 composites, which can pose a leakage risk at high fields, BN retains electrical insulation even at high temperatures.

Additionally, pure PAM remains at the lower end of the conductivity spectrum due to its amorphous structure and strong phonon scattering, which limit heat transport. While this restricts its use in heat-dissipating applications, it positions PAM as an effective baseline insulator whose performance can be significantly tuned through filler incorporation [3, 5].

Most state-of-the-art studies summarized in Table 4 focus on material-level thermal enhancement without establishing a direct link to photovoltaic device performance with passive polymeric layers. Instead, they showcase system-level electrical efficiency improvement. By incorporating effective composite thermal characteristics into a system-level FEM model of a PV/BIPV setup, this work closes this gap and allows to directly quantify temperature reduction and related efficiency gain. The $PAM - BN$ combination shows how the creation of continuous phonon-transport channels, which are absent in systems filled with amorphous oxide, results in quantifiable improvements in solar

performance. The $PAM-BN$ system achieves a higher passive efficiency improvement while maintaining dielectric safety and lower filler loading, in contrast to oxide-filled systems like Al_2O_3 –based composites reported in [27], which usually yield electrical efficiency gains below 0.4% at comparable effective conductivities. It should be highlighted that only in cases where direct PV-level thermal–electrical coupling was assessed are efficiency increases reported, and literature data for other composite systems is limited to material-level thermal performance and cost considerations.

SUMMARY AND CONCLUSION

Polymeric composites $PAM-SiO_2$ can be utilized as insulating layers in multilayer energy-management systems because of their customizable thermal behaviour.

As a beginning, H1 is verified: because of its greater effective thermal conductivity and more effective through-thickness heat transmission, the $PAM-BN$ composite layer lowers the silicon cell operating temperature in comparison to $PAM-SiO_2$. According to COMSOL models, $PAM-BN$ results in an average cell temperature reduction of 1.3 K. Under the same irradiation conditions, this directly translates into an increase in electrical efficiency of 0.66% (absolute +0.00114). This finding demonstrates that PV electrical performance is significantly impacted by improved heat conduction and decreased interfacial resistance in BN-filled systems.

H2 is verified as well. $PAM-SiO_2$ maximizes thermal energy retention by reducing downward heat flux, whereas $PAM-BN$ increases electrical output through improved heat evacuation. The observed decrease in retained energy by 4.8 $W\cdot m^{-2}$ in the $PAM-BN$ configuration can be explained quantitatively by the increased thermal conductivity of BN, which increases downward heat movement by 18 $W\cdot m^{-2}$ when compared to $PAM-SiO_2$. This compromise indicates that while $PAM-BN$ supports performance-oriented PV systems where electrical efficiency matters, $PAM-SiO_2$ is more appropriate for insulation-oriented systems.

The transient and through-thickness simulations align with H3. Corresponding to the presence of more continuous paths for phonon conduction, $PAM-BN$ exhibits smoother temperature gradients and faster thermal equilibration across the multilayer stack. Conversely, increased phonon scattering at interfaces reduces the rate of heat transfer. It also leads to localized energy trapping. $PAM-SiO_2$ retains sharper temperature gradients. These predictions agree with the latest understanding of phonon-transport in high-conductivity ceramic fillers such as BN.

By measuring a passive electrical efficiency gain (0.66%) using a thin polymeric composite layer without depending on active cooling, nanofluid circulation, or auxiliary power consumption, which are frequently reported in PV/T systems. The current study advances current knowledge when compared to the state of the art. Studies in the literature indicate that actively cooled PV/T combinations exhibit higher absolute electrical efficiency; however, these improvements are achieved at the expense of increased energy input and system complexity. For building-integrated applications, on the other hand,

where dependability and simplicity are crucial, the $PAM - BN$ layer offers a scalable, low-complexity substitute.

From a scalability and materials-design standpoint, the results indicate that hybrid filler strategies represent a clear extension beyond the current state of the art. Combining BN with low-cost insulating fillers such as SiO_2 offers a road to intermediate thermal conductivities. This helps to overcome the challenges of dispersion and the cost constraints. It also allows application-specific tuning of heat spreading and energy retention. These hybrid systems address the scalability and manufacturability gaps that were found in the recent SOTA literature on the polymer-based PV thermal management layers.

In general, this study represents an advancement of the state of the art because it goes beyond either purely insulating or purely conductive polymer composites. It also offers a quantitative, mechanism-based guide for designing composite layers that trade off heat dissipation, energy storage, and photovoltaic performance.

Future work may extend these findings through 3D modelling, inclusion of radiative heat-transfer effects, and coupled mechanical–thermal assessments to further evaluate long-term stability and manufacturability. Within this context, the present study provides a quantitative and mechanistic framework for selecting and engineering polymeric composite layers that bridge the gap between thermal insulation and heat dissipation in photovoltaic and solar-energy systems.

AUTHOR CONTRIBUTIONS

Conceptualization: A.H., and A.Q.; Methodology: A.H., and A.Q.; Formal analysis and investigation: A.Q.; Writing - original draft preparation: A.Q.; Writing - review and editing: A.Q.; Supervision: A.H.

CONFLICT OF INTERESTS

The authors confirm that there is no conflict of interest associated with this publication.

REFERENCES

1. Wang, Z., Wu, Z., Weng, L., Ge, S., Jiang, D., Huang, M., Mulvihill, D. M., Chen, Q., Guo, Z., Jazzar, A., He, X., Zhang, X., Xu, B. B. A Roadmap Review of Thermally Conductive Polymer Composites: Critical Factors, Progress, and Prospects. *Adv. Funct. Mater.* **2023**, *33*(36), 2301549
2. Kazem, H.A., Chaichan, M.T., Al-Waeli, A.H., Sopian, K., Alnaser, N.W., Alnaser, W.E. Energy Enhancement of Building-Integrated Photovoltaic/Thermal Systems: A Systematic Review. *Sol. Compass* **2024**, *12*, 100093.
3. Zhang, Y., Lv, Z., Lv, W., Zhang, K., Lei, Y., Huang, Y. Effects of Varying SiO_2 Content on the Superhydrophilic Properties of PAM/CSn Semi-IPN Hydrogels and Their Applications in Oil–Water and Emulsion Separation. *J. Water Process Eng.* **2024**, *68*, 106609.
4. Zhu, W., Zheng, G., Cao, S., He, H. Thermal Conductivity of Amorphous SiO_2 Thin Film: A Molecular Dynamics Study. *Sci. Rep.* **2018**, *8*(1), 10537.

5. Wang, H., Li, C., Wei, X., Li, J., Jia, C., Wang, B., Qi, X., Hu, P., Ying, Y., Tian, M. Design of SiO_2–TiO_2–PAM Composite Flocculant with Self-Degrading Characteristics and Optimisation of the Flocculation Process Using a Combination of Central Composite Design and Response Surface Methodology. *Colloids and Surfaces A: Physicochemical and Engineering Aspects* **2019**, *583*, 123982.
6. Cui, W., Du, F., Zhao, J., Zhang, W., Yang, Y., Xie, X., Mai, Y.W. Improving Thermal Conductivity While Retaining High Electrical Resistivity of Epoxy Composites by Incorporating Silica-Coated Multi-Walled Carbon Nanotubes. *Carbon* **2011**, *49*(2), 495–500.
7. Kou, R., Zhong, Y., Kim, J., Wang, Q., Wang, M., Chen, R., Qiao, Y. Improved Window Energy Efficiency with Thermal Insulating Polymer–Air Multilayer. *Appl. Therm. Eng.* **2021**, *191*, 116890.
8. Wang, N., Zhou, H., Ren, J., Gao, G., Zhao, G., Yang, Y., Wang, H., Wang, J. Polymer@SiO_2 Core–Shell Composite Particles: Preparation and Application. *Coatings* **2023**, *13*(2), 334.
9. Sonowal, J., Naik, B. K., Lakshmi, D., Muthukumar, P., Anandalakshmi, R. Evolution of Solar-Driven Desiccant Systems for Energy-Efficient Air Conditioning: A Review. *Sol. Compass* **2025**, 100115.
10. Kumar, D., Ganat, T., Lashari, N., Ayoub, M. A., Kalam, S., Chandio, T. A., Negash, B. M. Experimental Investigation of GO-HPAM and SiO_2-HPAM Composite for cEOR: Rheology, Interfacial Tension Reduction, and Wettability Alteration. *Colloids and Surfaces A: Physicochemical and Engineering Aspects* **2021**, *637*, 128189.
11. Fraleoni-Morgera, A., Chhikara, M. Polymer-Based Nano-Composites for Thermal Insulation. *Adv. Eng. Mater.* **2019**, *21*(7), 1801162.
12. Rahman, M.A., Gupta, S.K., Akylbekov, N., Zhapparbergenov, R., Hasnain, S.M.M., Zairov, R. Comprehensive Overview of Heat Management Methods for Enhancing Photovoltaic Thermal Systems. *iScience* **2024**, *27*(10), 110950.
13. Dai, Y., Bai, Y. Performance Improvement for Building Integrated Photovoltaics in Practice: A Review. *Energies* **2020**, *14*(1), 178.
14. Kwon, Y., Park, J., Jeon, Y., Hong, J., Park, H., Lee, J. A Review of Polymer Composites Based on Carbon Fillers for Thermal Management Applications: Design, Preparation, and Properties. *Polymers* **2021**, *13* (8), 1312.
15. García-Hernández, Z., Molina-Ramírez, O., Rivera-Salinas, J. E., Sifuentes-Nieves, I., González-Morones, P., Hernández-Hernández, E. Boron Nitride: The Key Material in Polymer Composites for Electromobility. *Polym. Compos.* **2024**, *46*(3), 1976–2029.
16. Li, M., Han, S., Dan, C., Wu, T., You, F., Jiang, X., Wu, Y., Dang, Z. Boron Nitride–Polymer Composites with High Thermal Conductivity: Preparation, Functionalization Strategy and Innovative Structural Regulation. *Small* **2025**, *21*(20), e2412447.
17. Mehdipour, M., Doğan, S., Al-Nadhari, A., Bafqi, M. S. S., Beylergil, B., Yildiz, M., Okan, B. S. Influence of Functionalized h-BN Particle Interphase and Interface Regulation with Structural Design on the Directional Thermal Conductivity and Mechanical Performance of Carbon Fiber/Epoxy Composites. *Composites Part A: Applied Science and Manufacturing* **2025**, *190*, 108708.
18. Wang, X., Wang, L., Su, Q., Zheng, J. Use of Unmodified SiO_2 as Nanofiller to Improve Mechanical Properties of Polymer-Based Nanocomposites. *Compos. Sci. Technol.* **2013**, *89*, 52–60.

19. Li, H., Cheng, B., Gao, W., Feng, C., Huang, C., Liu, Y., Lu, P., Zhao, H. Recent Research Progress and Advanced Applications of Silica/Polymer Nanocomposites. *Nanotechnol. Rev.* **2022**, *11*(1), 2928–2964.
20. Hwang, J., Kim, Y., Park, J., Rie, D. A Study on the Evaluation of Thermal Insulation Performance of Cellulose-Based Silica Aerogel Composite Building Materials. *Polymers* **2024**, *16*(13), 1848.
21. COMSOL. *Heat Transfer Module User's Guide*, Version 5.6; COMSOL AB, 2021. Available from: https://doc.comsol.com/5.6/doc/com.comsol.help.heat/HeatTransferModuleUsersGuide.pdf. (Access date: 11 September 2025)
22. Khalifa, A.N. Natural convective heat transfer coefficient – a review: I. Isolated vertical and horizontal surfaces. *Energy Convers. Manage.* **2001**, *42*(4), 491–504.
23. Zhang, L., Deng, H., Fu, Q. Recent Progress on Thermal Conductive and Electrical Insulating Polymer Composites. *Compos. Commun.* **2018**, *10*, 140–150.
24. Qamili, A., Kapia, S. Evaluation and Integration of Photovoltaic (PV) Systems in Albanian Energy Landscape. *Sol. Compass* **2024**, *10*, 100070.
25. Qamili, A., Hoxha, A. Thermal and Electrical Conductivity of Hybrid Epoxy Composites with Multi-Filler Systems: A Simulation Approach. In *Proceedings of the 7th International Mediterranean Congress*; University of Valencia, Spain, January 9–11, **2025**, pp. 886-896.
26. Peiyao, Q., Shuo, W., Ye, J., Zhongli, T., Jin, Q., Junping, Z., Xiaofei, L. Synthesis and Rheological Properties of Polyacrylamide Nanospheres and SiO_2/PAM Composite Nanospheres. *ChemistrySelect* **2022**, *7*(47), e202200923.
27. Ouyang, Y., Bai, L., Tian, H., Li, X., Yuan, F. Recent Progress of Thermal Conductive Polymer Composites: Al_2O_3 Fillers, Properties and Applications. *Composites Part A: Applied Science and Manufacturing* **2022**, *152*, 106685.
28. Dhoska, K., Spaho, E., Sinani, U. Fabrication of Black Silicon Antireflection Coatings to Enhance Light Harvesting in Photovoltaics. *Eng* **2024**, *5*, 3358-3380.

Appendix A. Numerical Model Definition

A1. Geometry Overview

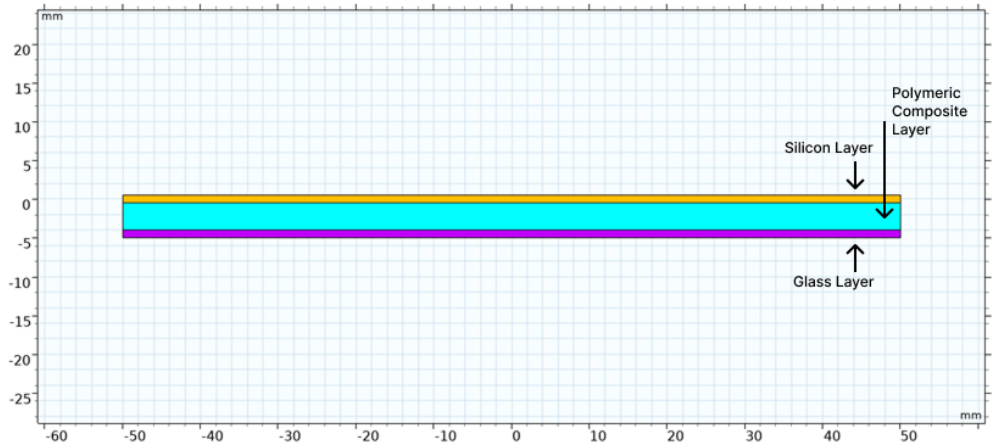

Figure 10. Layered Panel Geometry

A2. Materials and Properties

Table A1. Thermal and Environmental Parameters Applied in the Model

Property	Value (Glass)	Value (Si)	Value (PAM/BN)	Value (PAM/SiO_2)	Unit
ϱ	2300	2330	2110	2110	kg/m^3
Cp	700	700	950	950	J/(kg·K)
k	1.1	148	1.5–3	0.25–0.55	W/(m·K)
G	—	—	600–1000	600–1000	W/m^2
h	—	—	10	10	$W/(m^2·K)$
T_{amb}	—	—	25	25	°C
t	—	—	600	600	s

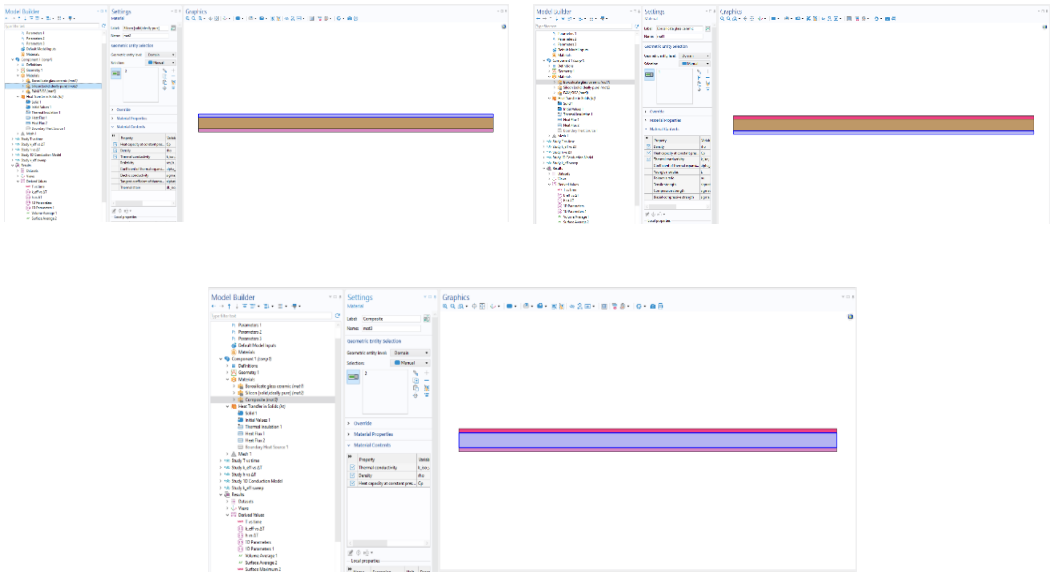

Figure 11. Material Selection

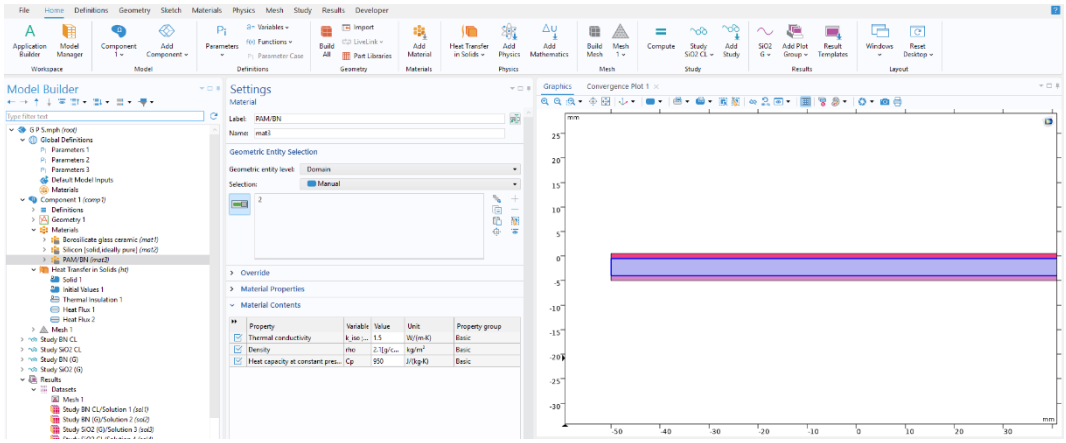

Figure 12. PAM/BN material selection

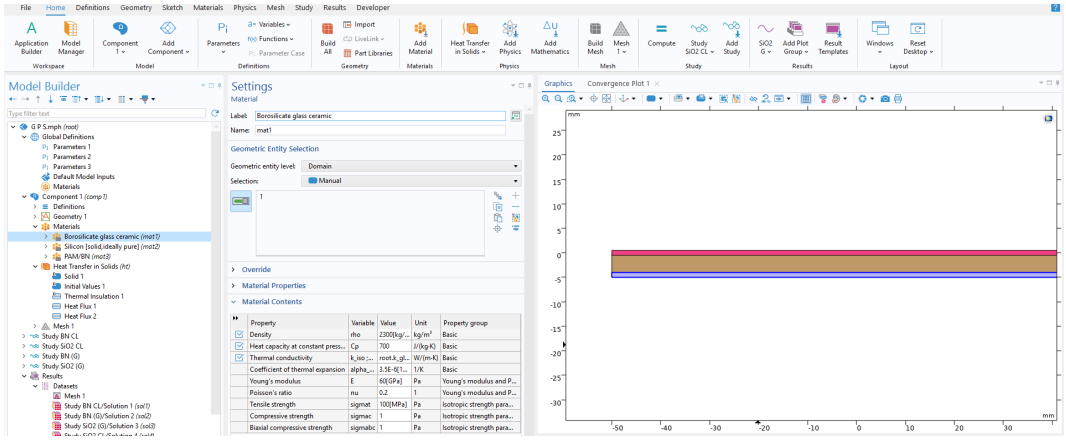

Figure 13. Glass material selection

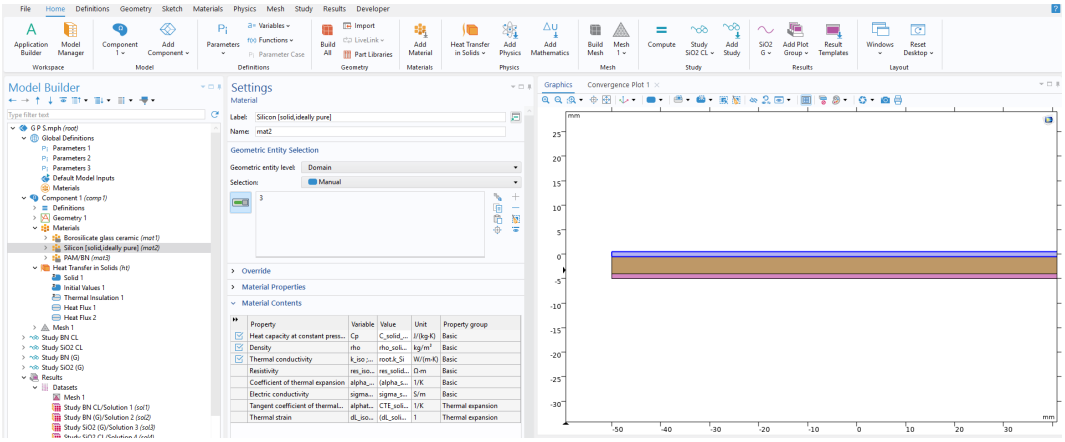

Figure 14. Silicon material selection

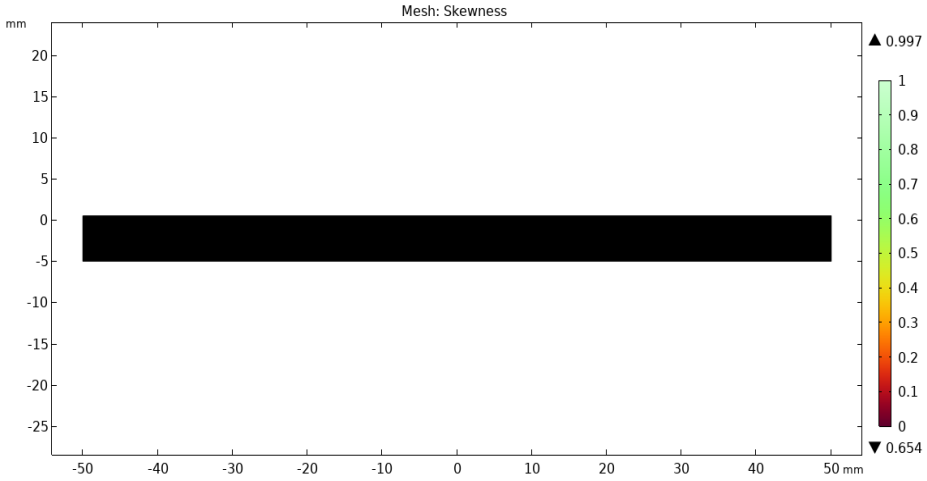

Figure 15. Mesh Skewness Plot

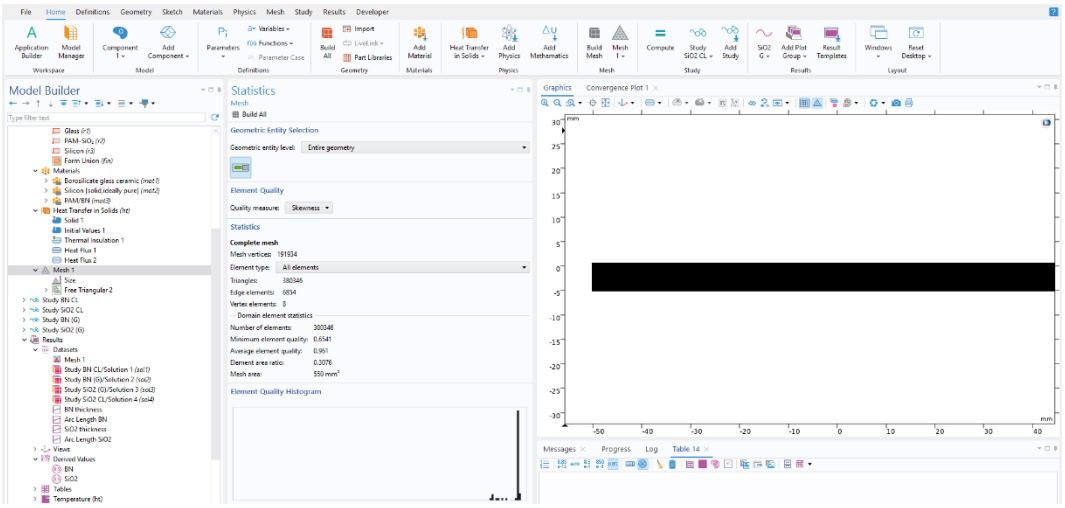

Figure 16. Mesh Properties

A3. Boundary Conditions

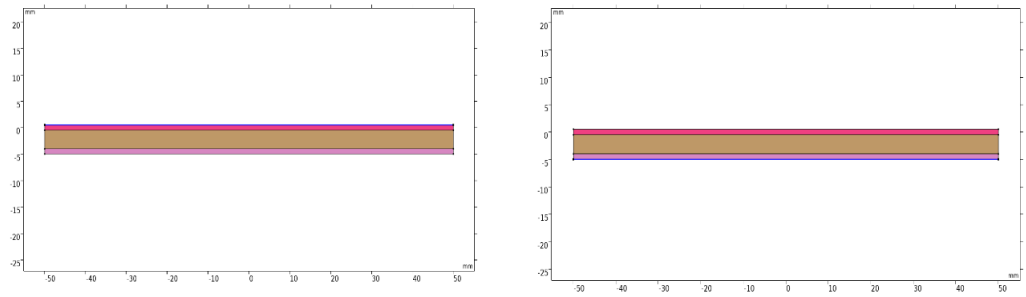

Figure 17. Boundary Conditions (top heat flux and bottom heat flux)

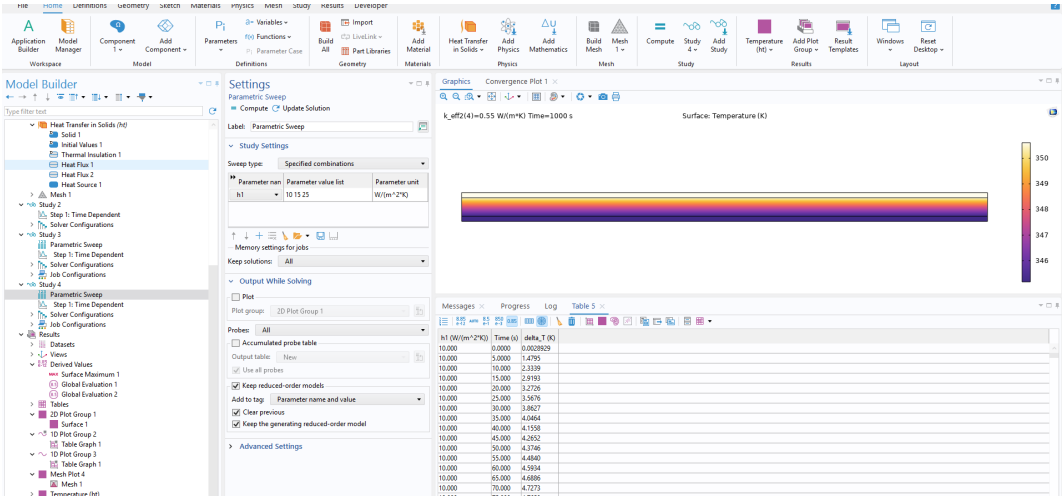

Figure 18. Parametric Sweep for h

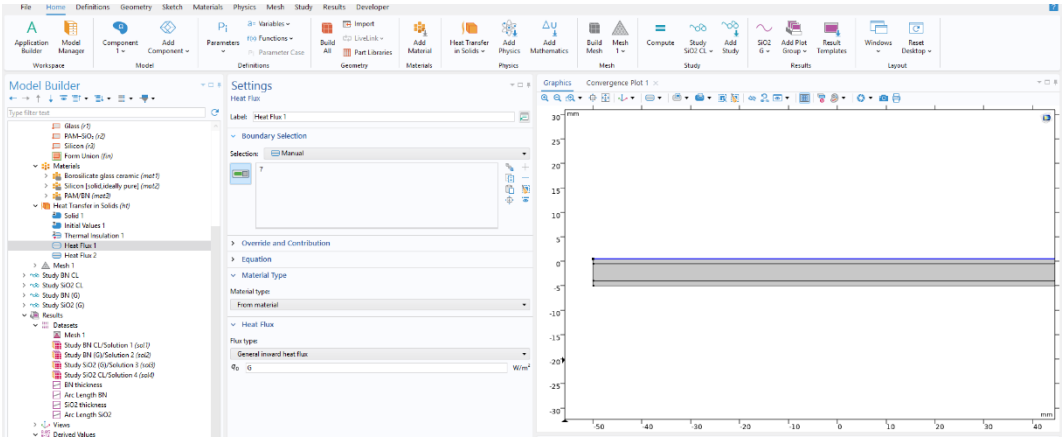

Figure 19. Applied Solar Irradiance Boundary Condition (Top Surface)

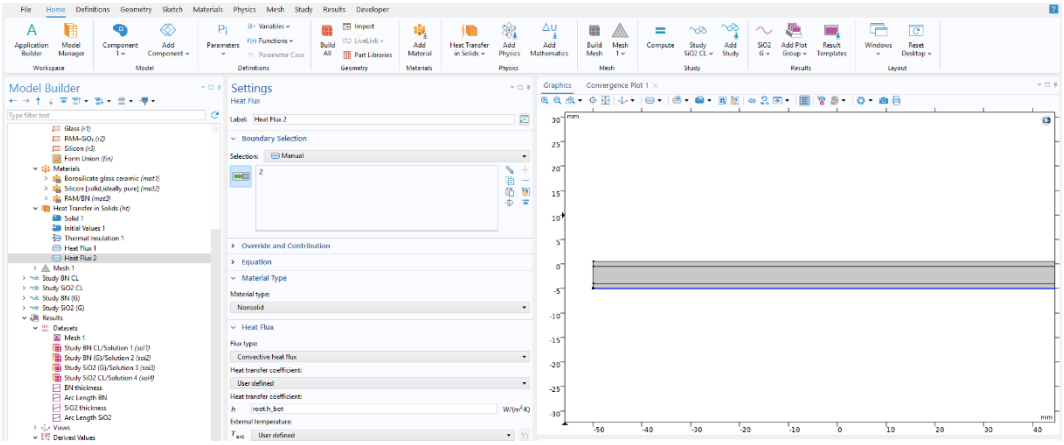

Figure 20. Convective Heat Transfer Boundary Condition (Bottom Surface)

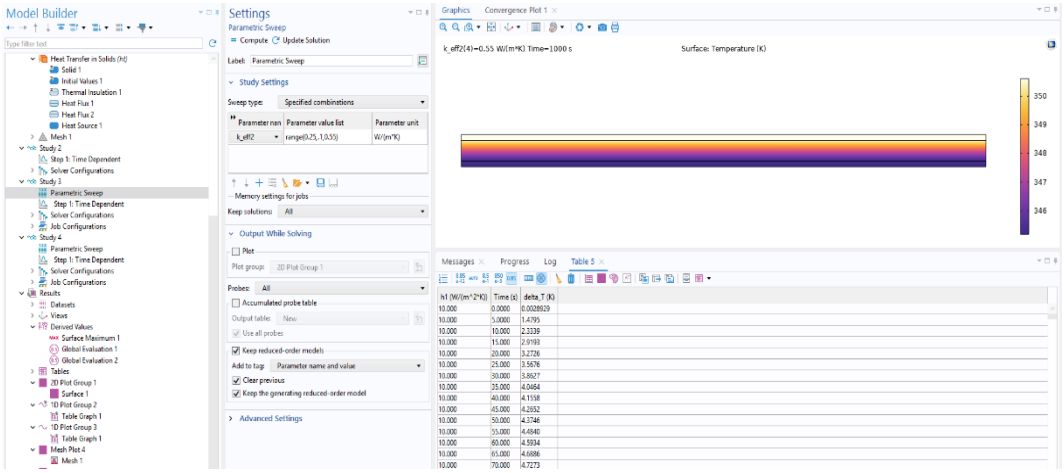

Figure 21. Parametric Sweep for k_{eff}

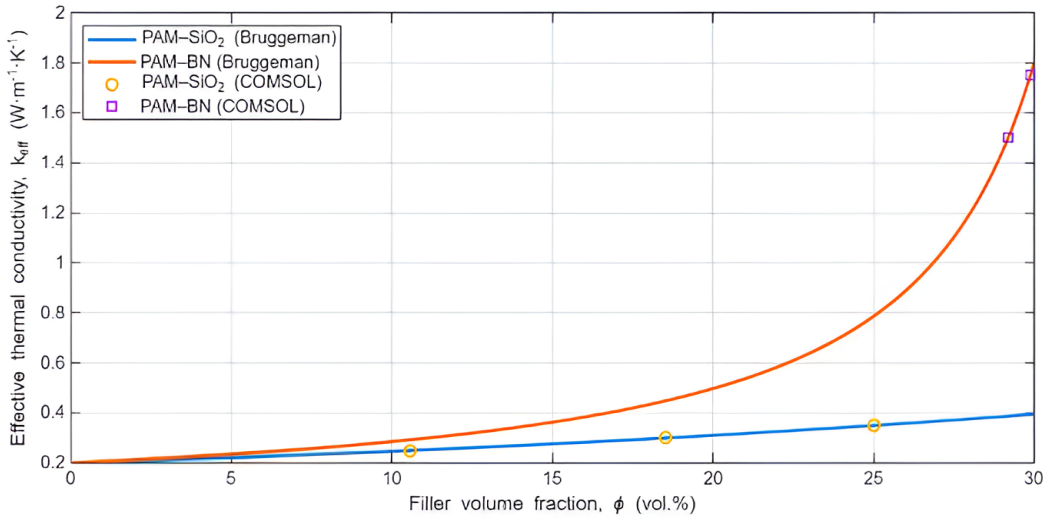

Figure 22. Bruggeman effective medium predictions of the effective thermal conductivity as a function of filler volume fraction for PAM–BN and PAM–SiO_2 composites, with markers indicating the effective conductivity values used in the COMSOL parametric study.

A physically interpretable foundation for the effective conductivity values used in the numerical simulations is provided by Tables A2–A4, which summarize the Bruggeman-based relationship between filler volume fraction and effective thermal conductivity for PAM–SiO_2 and PAM–BN systems.

Table A2. Bruggeman-predicted effective thermal conductivity as a function of filler volume fraction for PAM–SiO_2 composites (Matrix thermal conductivity k_m = 0.20W·m^{-1}·K^{-1}; amorphous SiO_2 filler)

Filler volume fraction, φ (vol.%)	**Effective thermal conductivity, k_{eff}(W·m^{-1}·K^{-1})**
0.0	0.20
5.0	0.26
10.0	0.26
10.5	0.30
20.0	0.35
25.0	0.42
30.0	0.50

Table A3. Bruggeman-predicted effective thermal conductivity as a function of filler volume fraction for PAM–BN composites (Matrix thermal conductivity k_m=0.20 W·m^{-1}·K^{-1}; h-BN filler)

Filler volume fraction, φ (vol.%)	**Effective thermal conductivity, k_{eff}(W·m^{-1}·K^{-1})**
0.0	0.20
1.0	0.28
2.0	0.38
3.0	0.55
5.0	0.85
10.0	1.60
15.0	2.40

Table A4. Effective thermal conductivity values used in the COMSOL parametric study and their qualitative interpretation

COMSOL k_{eff} (W·m^{-1}·K^{-1})	**Corresponding filler regime (Bruggeman-based interpretation)**
0.25-0.35	Low SiO_2 loading / very low BN loading
0.40-0.55	Moderate SiO_2 loading
1.50-2.00	Moderate BN loading
2.50-3.00	Upper-bound BN loading (analytical EMT regime)